Smart Structures and Systems, *Vol. 19, No. 1 (2017) 57-66*
DOI: https://doi.org/10.12989/sss.2017.19.1.057

Modelling of the interfacial damping due to nanotube agglomerations in nanocomposites

Chetan S. Jarali[*1], M. Madhusudan[2,3], S. Vidyashankar[3] and Y. Charles Lu[4]

[1]*Structural Technologies Division, CSIR National Aerospace Laboratories, Bangalore -560017, India*
[2]*Ph.D. Research Centre, Visvesvaraya Technological University, Belgaum-590008, India*
[3]*Department of Mechanical Engineering, Bangalore Institute of Technology, Bangalore -560004, India*
[4]*Department of Mechanical Engineering, University of Kentucky, Lexington, KY 40506, USA*

(Received May 26, 2016, Revised October 12, 2016, Accepted November 16, 2016)

Abstract. Nanocomposites reinforced with carbon nanotube fibers exhibit greater stiffness, strength and damping properties in comparison to conventional composites reinforced with carbon/glass fibers. Consequently, most of the nanocomposite research is focused in understanding the dynamic characteristics, which are highly useful in applications such as vibration control and energy harvesting. It has been observed that those nanocomposites show better stiffness when the geometry of nanotubes is straight as compared to curvilinear although nanotube agglomeration may exist. In this work the damping behavior of the nanocomposite is characterized in terms of loss factor under the presence of nanotube agglomerations. A micro stick-slip damping model is used to compute the damping properties of the nanocomposites with multiwall carbon nanotubes. The present formulation considers the slippage between the interface of the matrix and the nanotubes as well as the slippage between the interlayers in the nanotubes. The nanotube agglomerations model is also presented. Results are computed based on the loss factor expressed in terms of strain amplitude and nanotube agglomerations. The results show that although – among the various factors such as the material properties (moduli of nanotubes and polymer matrix) and the geometric properties (number of nanotubes, volume fraction of nanotubes, and critical interfacial shear stresses), the agglomeration of nanotubes significantly influences the damping properties of the nanocomposites. Therefore the full potential of nanocomposites to be used for damping applications needs to be analyzed under the influence of nanotube agglomerations.

Keywords: numerical material modeling; nanocomposites; damping; hysteresis, agglomeration

1. Introduction

Carbon materials at nanoscales are drawn as nanotubes (CNTs), which show extraordinary properties and hence have been extensively used as fillers in clay, epoxy resins, metal and cement matrices to develop composites for damping applications (Fereidoon, Kordani *et al.* 2010, Deng, Wang *et al.* 2007, Kireitseu, Hui *et al.* 2008). CNTs exhibit excellent elastic properties, extremely high aspect ratios, and excellent electrical and thermal conductivity properties as shown by Salvetat and Rubio (2002), Esawi and Farag (2007), Paradise and Goswami (2007). As a result, CNTs are excellent fillers to develop multifunctional composites for various engineering and science applications, specifically for damping. (Brackbill, Lesieutre *et al.* 2000, Wetzel, Rosso *et al.* 2006) and Lindler and Wereley (1999) have carried out extensive works to investigate the damping properties of thermoset, thermoplastic, elastomer and rheological materials using nano inclusions. At nano scale geometry, nanotubes possess very good dynamic properties because of their ultra-low densities of the nanotubes and significantly high surface areas and surface energies. Therefore CNTs are ideal substitutes in multifunctional composites to be used in high damping applications (Koratkar, Wei *et al.* 2002). These features have resulted in better energy dissipation and structural damping. The advantage of good interfacial friction contact between the CNTs and matrix is the key mechanism in such applications. Generally, damping in nanocomposites is computed by estimating the storage modulus, loss modulus and their ratio (loss factor). Rajoria and Jalili (2005) have observed good damping in case of multiwalled carbon nanotubes (MWCNTs) by using 3-5wt% of CNTs in polymer/clay matrices. Some studies show that a 2wt% of single walled carbon nanotubes (SWCNTs) in polymer resin has contributed to the increase in the loss modulus of the nanocomposite up to 1000% (Koratkar, Wei *et al.* 2002). The works of (Ajayan, Suhr *et al.* 2006) and Suhr and Koratkar (2008) show that a strong dependency of strain-amplitude relationship is evident in the estimation of the damping behavior of SWCNT polycarbonate nanocomposite. Further, it is observed that nanotube agglomeration shows increased damping characteristics because of large interfacial area available for the slippage. The modelling studies which have incorporated interfacial 'stick-slip' concept, have neglected the CNT agglomeration influence on the damping. Therefore, the realistic effect of the influence of agglomeration especially for the damping studies is not

[*]Corresponding author, Ph.D.
E-mail: chetan.jarali@gmail.com

ISSN: 1738-1584 (Print), 1738-1991 (Online)

considered. A potential research problem is emerging in order to understand the damping phenomena under CNT agglomerations. In this direction, a stick-slip model is proposed and the damping properties are computed, which are validated by experimental results (Zhou, Shin *et al*. 2004). Further, stick-slip models are also used to investigate the load transfer mechanism in nanocomposites (Liu, Huang *et al.* 2006, Liu, Wang *et al.* 2010). Lin and Lu (2010) also developed a stick-slip damping model based on micromechanics approach that considers the interfacial slips between the matrix and CNTs and between the individual walls of CNTs for MWCNT nanocomposites. Buldum and Lu (1999) employed molecular dynamics simulation approach by incorporating the nanotube wall slippages, interfacial sliding and rolling of CNTs in the resin. The interfacial stick-slip mechanism is based on the understanding that CNTs transfer better load under initial loading up to the point where the CNTs start to slip between the walls. Li and Chou (2003) has observed that as strain increases the rate of slippage progresses at much faster rate thus releasing the external load. It is concluded that bonding force between the resin and the CNT fillers is higher than the van der Waal forces acting at interface of CNTs. Sun and Lu (1995) used the loss factor to calculate damping in nanocomposites both analytically as well as experimentally. Free and forced vibration tests are also performed on nanocomposites containing carbon fibers as hybrid reinforcements in order to characterize the damping (Khan, Li *et al*. 2011, Jarali, Patil *et al*. 2015). The experimental study is able to prove that nanotube content significantly increases the damping in composites as compared to composites with conventional carbon fibers. The mechanism of interfacial slippage between the CNT walls has been analyzed using Scanning Electron Microscope (SEM) by (Yu, Yakobson *et al*. 2000). Stick-slip motion between the CNT walls has been observed and a damping model based on the interfacial shear stress transfer has been applied to study the sliding between the CNT walls. It has been observed that the bonding among the CNTs and the resin system is much higher than the bonding between the CNT walls. This understanding has been substantiated by the molecular dynamics simulation as well as micromechanics study by (Xu, Thwe *et al*. 2002). The previous works suggest that MWCNTs possess excellent mechanical properties, chemical stability, and ease of manufacturing and moderate cost in comparison to SWCNTs. As a result, MWCNTs are potentially being used to develop CNT nanocomposites. Basically, the models for damping studies are based on the understanding that when low stress is applied (less than critical shear stress, the CNTs and resin system are intact (sticking phase), and deform as a single system due to the interfacial stress transfer phenomena (Gou, Minaie *et al*. 2004, Arash, Jafar *et al.* 2010, Geng, Liu *et al.* 2008). Further increase in the load increases the interfacial shear stress between the walls of the nanotubes resulting in additional deformations of the matrix and the nanotubes. At the point of the critical shear stress debonding between the nanotubes and the matrix is observed. Further application of load results in inducing constant strain in the nanotubes, while strain in the matrix increases causing slipping at the debonded regions (slipping phase). Consequently, there may be energy dissipation due to the slippage between the matrix and the nanotubes, which leads to increase in the damping. Therefore it is required that there is a need to characterize the damping of SW/MW CNT nanocomposites by taking into account the agglomeration effects (Arash, Jafar *et al*. 2010, Jarali, Patil*et al.* 2013).

As a result, the present work extends the previous work by Lin and Lu (2010**)** by further improving the analytical procedure with using stick-slip procedure to predict the damping of MWCNT nanocomposites with agglomerations. Additionally, it is also focused to estimate the loss factor in terms of the strain amplitude for the MWCNT composites by using a RVE model that accounts for the CNT agglomerations. A further consideration of the slippage initiation at the outermost layer of CNTs and surrounding resin system as well as within the neighboring layers of CNTs has been included in the study. The slippage mechanism is essential for the damping model, which is supported by experimental observations of the proposed slippage sequences. Also the slip-stick depends on the slenderness and critical length of the nanotubes used, and therefore the dependence on the overall stiffness that contribute for damping has been considered in the present work. Finally, in the present work the interfacial strengths reported from the experimental results have been employed in the analytical model. The results derived from the current model are based on the experimental data for the induced shear stresses at the interface. The results are computed based on the CNT strain dependent behavior, which may be easily applied to a variety of static and dynamic applications including damping of structures.

2. Damping model for MWCNT polymer nanocomposite

The previously discussed interfacial stick-slip procedure is adopted in the damping model. An assumption is made that nano fillers are straight and not having any curvature, near perfect bonding, directionally aligned and in a state of high and low agglomerations (Jarali, Patil *et al.* 2013, Jarali, Basavaraddi *et al*. 2014).

In the model formulation a generalization is done for MWCNTs with n layers. The composite unit cell is represented as a circular cylinder consisting of matrix with circular cross sectional CNTs. Nanotubes are concentric with the central axis of the matrix as shown in Fig. 1. Consequently the interfacial damping with agglomerations of CNTs has been considered, with each wall of CNTs considered to be deforming elastically.

However, the viscoelastic losses of the CNTs and the matrix have been neglected. In the RVE it may be assumed that each layer of CNTs as well as the matrix be individual inclusions, which represent springs in parallel arrangement as shown in Fig. 2.

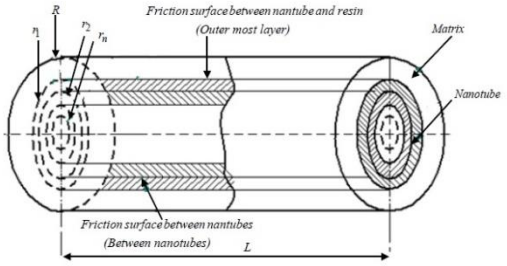

Fig. 1 Representative volume element for the MWCNT-polymer composite.

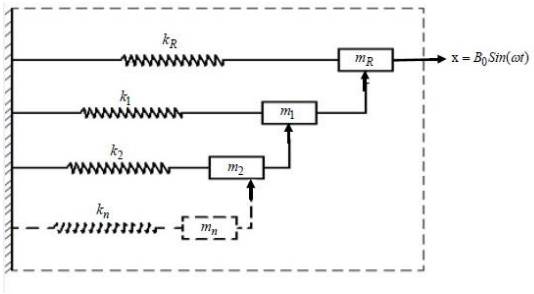

Fig. 2 Representative volume element for damping model

$k_{1,..n}$ represent the stiffness of the nanotube and $m_{1,..n}$ the mass of the nanotube. k_R and m_R define the stiffness and mass of the resin system. The elastic stiffness of the matrix k_m^P may be written as

$$k_m^P = \frac{A_m^P E_m^P}{L} \tag{1}$$

where, A_m^P and E_m^P are the cross-sectional area and the elastic modulus of the polymer matrix containing the MWCNT, respectively, and L is the length of the RVE (unit cell). The area of the polymer matrix in the RVE can be defined as

$$A_m^P = \pi(R^2 - r_1^2) \tag{2}$$

where the radius of the RVE is defined by *R* and r_1 is the outermost radius of the MWCNT. The volume fraction of the MWCNTs in the RVE V_f^C can be proposed to be

$$f_t^N = \frac{(Volume\,of\,the\,CNT\,in\,the\,RVE)}{(Volume\,of\,the\,RVE)} = \frac{(\pi_f^C r_1^2 L_f^C)}{\pi R^2 L} \tag{3}$$

where L_f^C is the average critical length of the CNTs, which is considered in the present work due to the physical importance of the slip-stick mechanism depending on the slenderness and critical length of the nanotubes used. Using Eq. (3), the radius of the RVE can be simplified as

$$R = \frac{r_1}{\sqrt{f_t^N}} \tag{4}$$

From the total volume of the nanotubes (V_t^N), the volume fraction of the CNTs (f_t^N) that corresponds to the highly concentrated agglomeration regions can be formulated as the ratio of high concentration of nanotubes (V_h^N) in the agglomeration volumes to the total volume that represents the high agglomerations (V_c^N). The expression is mathematically written as (Jarali, Patil *et al*.2013)

$$\frac{V_h^N}{V_c^N} = \frac{\zeta_h^N V_t^N}{\xi_c^N V} = \frac{\zeta_h^N f_t^N}{\xi_c^N}. \tag{5}$$

where, (ξ_c^N) is the volume fraction of the agglomerated CNT regions (cylinders) with severe (ζ_h^N) or dilute (ζ_d^N) CNT agglomerations, respectively. Similarly, that volume of nanotubes which may not be dispersed so densely in the matrix can be represented as the total volume of dilute agglomerations. Consequently, this dispersion may lead to dilute accumulation of nanotubes within such regions/volumes (V_d^N). The corresponding volume fraction for regions containing the CNTs which are in dilute agglomeration can be obtained as (Jarali, Patil *et al*. 2013, Jarali, Basavaraddi *et al*. 2014)

$$\frac{V_d^N}{V - V_c^N} = \frac{f_t^N (1 - \zeta_h^N)}{1 - \xi_c^N}. \tag{6}$$

Therefore, the volume fraction of the polymer matrix (f_m^P) with volume (V_m^P) when the nanotubes are highly agglomerated, less agglomerated and also uniformly dispersed in some other regions is derived as

$$\frac{V_m^P}{V} = 1 - \frac{V_h^N + V_d^N}{V_c^N}. \tag{7}$$

Next carbon nanotube stiffness is given by

$$k_n = \frac{A_n E_f^C}{L_f^C} \tag{8}$$

where E_f^C is the Young's modulus of CNTs. The area of cross section for the nth layer of CNT, A_n, is expressed as

$$A_n = \pi(r_n^2 - (r_n - t)^2) \tag{9}$$

where t is the CNT wall thickness. Equations of deformation are written for all the number of nanotube walls as well as for the matrix. Expression relating the applied stress and the RVE deformation is then obtained. The general understanding is that the transfer of load between the matrix and the CNTs, and also in between the individual nanotubes is through the interfacial shear stress. Since the MWCNTs are hollow concentric cylinders, the CNTs have a very small cross sectional area when compared to the surface areas in the lateral directions. Therefore, the shear stress developed at the interface of CNT layers and between CNT and the matrix is the main

load transfer mechanism in the nanocomposites. As a result the contribution of normal stresses can be ignored. The interfacial shear stresses result in the axial deformation of the carbon nanotubes up to the point of critical shear stress, beyond which the stress acting on the nanotubes may not produce any further deformations (Zhou, Shin *et al*. 2004).

The critical shear stresses depend on the properties of the individual constituents that comprise the RVE. Therefore different values of critical shear stresses may exist between the matrix and nanotubes and in between nanotube layers. Considering the fact that the interface attachment among the CNTs and resin systems is higher than the van der Waal forces acting between the CNTs (Li and Chou 2003), in this work the shear stress distribution is defined as $\tau_1{}_P^N > \tau_2{}_t^N$. Here $\tau_1{}_P^N$ is the critical shear stress between the CNTs and the resin system and $\tau_2{}_t^N$ is the critical shear stress between the CNT walls. This relationship is an important assumption in developing the damping models for nanocomposites. Under the application of external load, both the matrix and CNT layers deform uniformly. As a result it may be assumed that the energy loss at such low strain amplitude levels is very small and may be neglected. As the deformation progresses, the shear force at the interface of nanotube and resin, and among the CNT walls may also increase, until the corresponding critical shear stresses have been reached. Accordingly, in this analysis it is considered that the most inside CNT layer slips first while the adjacent inner layers are in perfect bonding with the first inner layer. Therefore, the displacement of the first inner layer in relation to the outer layer of the deforming CNT is given by

$$\delta_1 = \frac{2\pi r_2 L \tau_1}{k_2 + k_3 + ... + k_{n-1} + k_n} \tag{10}$$

In addition, the displacement of the outermost layer is

$$\delta_2 = \frac{2\pi r_1 L \tau_2}{k_1} \tag{11}$$

For strain values higher than δ_1 during deformations of the first CNT inner layer in relation to the outer layer, there may be loss in the damping energy. In this case it may be assumed for the model developments that the outermost CNT layer and matrix are still in perfect bonding without any slippage. However as the strain value exceeds δ_2 sliding between the matrix and the most outside CNT layer may initiate as a next step in the deformation process. Finally, the deformation of the outermost layers may also cease. For the present case of the amplitude of vibration $(\delta_1 < \delta_2 < X)$, the following hysteresis loop is shown in Fig. 3. From Fig. 3 it should be understood that, when $x < \delta_1$, no slip occurs and the effective stiffness of the system is $(k_m^P + k_1 + k_2 + ... + k_n)$. As the amplitude of strain approaches and exceeds $\delta_1 (\delta_1 < x < \delta_2)$ at point (*P*), slippage between the CNT layers is initiated which means that k_2 starts to slip. Therefore, the effective stiffness will be $(k_R + k_1)$. For the deformation at point *Q* $(x \geq \delta_2)$, slip between the matrix and CNT outer layer is initiated. This means that k_1 starts to slip. Consequently the effective stiffness reduces to k_R and the vibration amplitude *X* is reached. At point *X*, there is a change in the direction of deformation, therefore force follows the line *R-S* with the effective stiffness as $(k_m^P + k_1 + k_2 + ... + k_n)$. Next as the deformation proceeds till point *T* the effective stiffness is $(k_R + k_1)$. The final stiffness of the nanocomposite is k_R when the deformation reaches the point U in the opposite direction. The deformation curve follows the paths *UV, VW* and *WQ* to define an entire cycle of one hysteresis loop. Further, the hysteresis cycle repeats following the sinusoidal displacement excitations. The equations of lines which represent to build the hysteresis loop for the multiwall carbon nanotubes are defined as follows

2.1 For the case when $(\delta_1 < \delta_2 < X)$

Slip of the CNT first inner layer (k_2) with respect to the outer CNT layer (k_1)

$$\begin{aligned}
&OP: F = y = (k_R + k_1 + ... + k_n)x \\
&PQ = TQ: F = y = (k_R + k_1)x + (k_2 + ... + k_n)\delta_1 \\
&QR =: F = y = k_R x + k_1\delta_2 + (k_2 + ... + k_n)(\delta_1) \\
&RS: F = y = (k_R + k_1 + ... + k_n)x + k_1(\delta_1 - X) + (k_2 + k_3 + ... + k_n)(\delta_1 - X) \\
&ST: F = y = (k_R + k_1)x + k_1(\delta_2 - X) - (k_2 + k_3 + ... + k_n)(\delta_1) \\
&UV: F = y = (k_R + k_1 + ... + k_n)x + k_1(X - \delta_2) + (k_2 + k_3 + ... + k_n)(X - \delta_1) \\
&VW: F = y = (k_R + k_1)x + k_1(X - \delta_2) + (k_2 + k_3 + ... + k_n)(\delta_1) \\
&WR: F = y = k_R x + k_1\delta_2 + (k_2 + k_3 + ... + k_n)(\delta_1)
\end{aligned} \tag{12}$$

The description for instance, when $(\delta_1 < x < \delta_2)$ can be explained similarly for which the hysteresis loop obtained is as shown in Fig. 4. The hysteresis curves are defined by the lines using the equations given below.

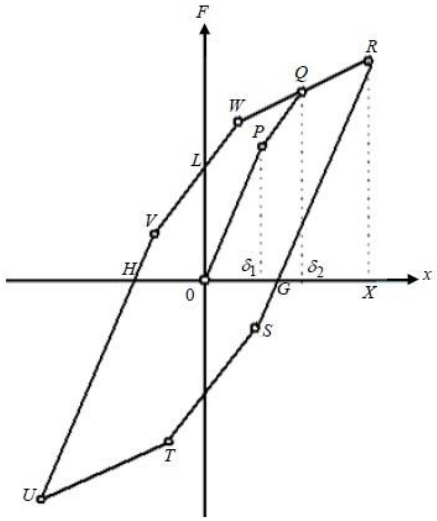

Fig. 3 Hysteresis loop of force-displacement for $\delta_1 < \delta_2 < X$.

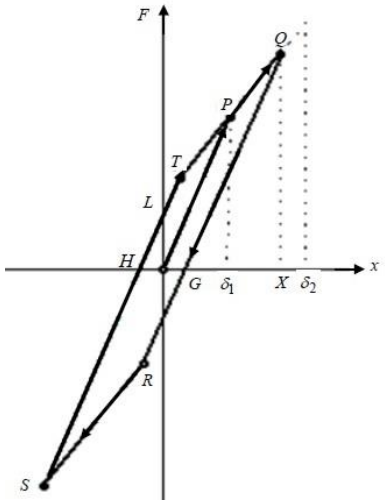

Fig. 4 Hysteresis loop of force-displacement for $\delta_1 < X < \delta_2$.

2.2 For the case

When $(\delta_1 < x < \delta_2)$

$$\begin{aligned}
&OP: F = y = (k_R + k_1 + \ldots\ldots + k_n)x \\
&PQ = TQ: F = y = (k_R + k_1)x + (k_2 + \ldots\ldots + k_n)\delta_1 \\
&QR =: F = y = (k_R + k_1 + \ldots\ldots + k_n)x + (k_2 + \ldots\ldots + k_n)(\delta_1 - X) \\
&RS: F = y = (k_R + k_1)x - (k_2 + k_3 + \ldots\ldots + k_n)(\delta_1) \\
&ST =: F = y = (k_R + k_1 + \ldots\ldots + k_n)x - (k_2 + \ldots\ldots + k_n)(\delta_1 - X)
\end{aligned} \quad (13)$$

The expressions representing the hysteresis curves may be using algebra in order to simulate the hysteretic behaviors. These hysteretic curves are used to obtain the displacement force relationships so that the loss factor can be computed. The loss factor (η) is usually defined as the ratio of the energy loss with respect to the total potential energy (U) that can be dissipated per cycle per radian (Sun and Lu 1995). The energy loss per cycle is known by the area within the hysteretic loop.

The loss factor is written as

$$loss\ factor(\eta) = \frac{area\ inside\ the\ hysteresis\ loop}{2\pi U} \quad (14)$$

Therefore, the areas represented by the hysteresis loop are computed using the equation of lines that represent the hysteretic curves. The total energy of hysteresis curve, for $(\delta_1 < \delta_2 < x)$, is

$$U = \frac{1}{2}k_R X^2 + \frac{1}{2}k_1(\delta_2)^2 + \frac{1}{2}(k_2 + \ldots\ldots + k_n)(\delta_1)^2 \quad (15)$$

The equations and coordinates representing the lines are used to determine the area inside the hysteresis loop. Therefore, the coordinates that define the lines as well as the points that intersect *x* and *y* axes are determined first by referring to the Fig. 3. The coordinates of the points that represent the lines are

$$\begin{aligned}
&P[\delta_1, (k_R + k_1 + \ldots\ldots + k_n)\delta_1] \\
&Q[\delta_2, (k_2 + \ldots\ldots + k_n)\delta_1 + (k_R + k_1)\delta_2] \\
&R[X, (k_2 + \ldots\ldots + k_n)\delta_1 + k_R X + k_1\delta_2] \\
&S[(X - 2\delta_1), (k_R X + k_1\delta_2 - 2k_R\delta_1 - 2k_1\delta_1 - (k_2 + \ldots\ldots + k_n)\delta_1] \\
&T[(X - 2\delta_2), (k_R X + k_1\delta_2 - 2k_R\delta_2 - (k_2 + \ldots\ldots + k_n)\delta_1] \\
&G[\frac{k_1(X - \delta_2) + (k_2 + \ldots\ldots + k_n)(X - \delta_1)}{(k_R + k_1 + \ldots\ldots + k_n)}, 0] = [g, 0] \\
&H[\frac{k_1(\delta_2 - X) + (k_2 + \ldots\ldots + k_n)(\delta_1 - X)}{(k_R + k_1 + \ldots\ldots + k_n)}, 0] = [h, 0] \\
&L[0, (k_1(X - \delta_2) + (k_2 + \ldots\ldots + k_n)\delta_1)] = [0, l]
\end{aligned} \quad (16)$$

The area under the hysteresis loop is computed by integration as

$$\begin{aligned}
A = 2&\left\{\int_h^{(2\delta_1 - X)} (Equation\ of\ line UV)\,dx + \int_{(2\delta_1 - X)}^{(2\delta_2 - X)} (Equation\ of\ line VW)\,dx\right\} \\
+ 2&\left\{\int_{(2\delta_2 - X)}^{X} (Equation\ of\ line WR)\,dx - \int_g^X (Equation\ of\ line RS)\,dx\right\}
\end{aligned} \quad (17)$$

$$\begin{aligned}
A = 2&\left\{\int_h^{(2\delta_1 - X)} ((k_R + k_1 + \ldots. + k_n)x + k_1(X - \delta_2) + (k_2 + k_3 + \ldots. + k_n)(X - \delta_1))\,dx\right\} \\
+ 2&\left\{\int_{(2\delta_1 - X)}^{(2\delta_2 - X)} ((k_R + k_1)x + k_1(X - \delta_2) + (k_2 + k_3 + \ldots. + k_n)\delta_1)\,dx\right\} \\
+ 2&\left\{\int_{(2\delta_2 - X)}^{X} (k_R x + k_1\delta_2 + (k_2 + k_3 + \ldots. + k_n)\delta_1)\,dx\right\} \\
-&\left\{\int_g^X ((k_R + k_1 + \ldots. + k_n)x + k_1(\delta_2 - X) + (k_2 + k_3 + \ldots. + k_n)(\delta_1 - X))\,dx\right\}
\end{aligned} \quad (18)$$

Next, consider that case when $\delta_1 < X < \delta_2$, the potential energy is defined as

$$U = \frac{1}{2}(k_R + k_1)X^2 + \frac{1}{2}(k_2 + \ldots\ldots + k_n)\delta_1^2 \quad (19)$$

The coordinates of points required for integration are computed from Fig. 4 and using Eq. (13) as, *O* (0,0)

$$\begin{aligned}
&P[\delta_1, (k_R + k_1 + \ldots\ldots + k_n)\delta_1] \\
&Q[X, (k_2 + k_3 + \ldots\ldots + k_n)\delta_1 + (k_R + k_1)X] \\
&R[(X - 2\delta_1), (k_R + k_1)X - 2k_R\delta_1 - 2k_1\delta_1 - (k_2 + \ldots\ldots + k_n)\delta_1] \\
&G[\frac{(k_2 + k_3 + \ldots\ldots + k_n)(X - \delta_1)}{(k_R + k_1 + \ldots\ldots + k_n)}, 0] = [g, 0] \\
&H[\frac{(k_2 + k_3 + \ldots\ldots + k_n)(\delta_1 - X)}{(k_R + k_1 + \ldots\ldots + k_n)}, 0] = [h, 0] \\
&L[0, (k_2 + k_3 + \ldots\ldots + k_n)(X - \delta_1)] = [0, l]
\end{aligned} \quad (20)$$

The area inside the hysteresis loop is

$$\begin{aligned}
A = 2&\left\{\int_h^{(2\delta_1 - X)} (Equation\ of\ line ST)\,dx + \int_{(2\delta_1 - X)}^{X} (Equation\ of\ line TQ)\,dx\right\} \\
- 2&\left\{\int_g^X (Equation\ of\ line QR)\,dx\right\}
\end{aligned} \quad (21)$$

$$A = 2\left\{\int_{h}^{(2\delta_1 - X)} ((k_R + k_1 + ... + k_n)x - (k_2 + ... + k_n)(\delta_1 - X))\,dx\right\} + 2\left\{\int_{(2\delta_1 - X)}^{X} ((k_R + k_1)x + (k_2 + ... + k_n)\delta_1)\,dx\right\} - 2\left\{\int_{g}^{X} ((k_R + k_1 + ... + k_n)x + (k_2 + ... + k_n)(\delta_1 - X))\,dx\right\} \quad (22)$$

In the present case the loss factor is computed in terms of the CNT properties, dimensions and agglomeration effects. Using various input parameters the strain amplitude dependent loss factor can be computed. The specification of input parameters is the key for the validity and accuracy of the present work.

3. Results and discussions

In the present work, the damping characteristics of the nanocomposites are studied in terms of loss factor with respect to the strain amplitudes. Constant strain amplitude of 0.0025 has been used to study the effects of CNT and matrix material properties, agglomeration influence on strain amplitude and also the direct effect of interfacial shear stress on the strain amplitude levels (Lin and Lu 2010). The material properties of the epoxy resin include the Young's modulus $E_m^P = 3.3GPa,$ and the density $\rho^m = 1200kg/m^3,$ The material property of the CNT includes the nominal Young's modulus $E_t^N = 650GPa,$ with a range of 500-1000 GPa (Salvetat and Rubio 2002, Esawi and Farag 2007, Lin and Lu 2010). The weight fractions of the CNTs are assumed to be 0.5% and 0.7% in the nanocomposites (Yu, Yakobson *et al.* 2000). The value of interfacial shear strength between the epoxy matrix and CNTs has been reported to be in the range of 35-376 MPa based on the fiber pullout tests (Xu, Thwe *et al*. 2002, Gou, Minaie *et al*. 2004).

3.1 Effect of weight percentage and CNT radius

The strain dependent loss factors of the nanocomposites are obtained, as shown in Figs. 5-15. In Fig. 5 the plots represent the variations in the loss factor for 0.5% CNT with 5 walls for vibration strain amplitude of 0.0025. In the case of no agglomeration (that is uniform dispersion of CNTs); it may be observed that as the CNT layers start slipping there is an increase in the loss factor. After the initial slippage between the subsequent layers, the shear stress transfer among the nanotube walls now eases as the amplitude of strain becomes high. As a result the axial load is now shared among the nanotube walls. As the strain amplitude becomes high the available potential energy that can be stored decreases, resulting in the decrease in the loss factor. This variation is also identical to the case with CNT agglomerations. As the strain amplitude progress beyond 0.2%, there is further slippage with stress transfer between the CNT walls and the epoxy matrix. As a result the loss factor also increases and then gradually decreases until the slippage between the CNT walls and the matrix stops. Fig. 6 shows the effect of CNT radius on damping property of the nanocomposites. It may be observed that with the increase in the outer radius of CNTs, the loss factor is considerably reduced for all the three cases: no agglomeration, low agglomeration and high agglomeration.

This means that as the interfacial distance between the CNT walls increases the CNT radius also increases. Consequently, the interfacial shear stress is not sufficient enough to cause the slippage between CNT walls resulting in lower storage of potential energy. As such it may be understood that the loss factor is reduced as the CNT radius is increased. The previous observations bring out an important point that the interfacial shear stress values to cause slippage should be higher as the outer radius of the CNT increases. The shear stress values required for the slippage should be less than the critical shear stresses, which result in the debonding of the CNT outer walls with the matrix. Moreover the interfacial shear stresses between the CNT walls should also be lower than the shear stress between the CNTs and the matrix. Now consider the agglomeration effect with agglomeration volume fraction being 50%.

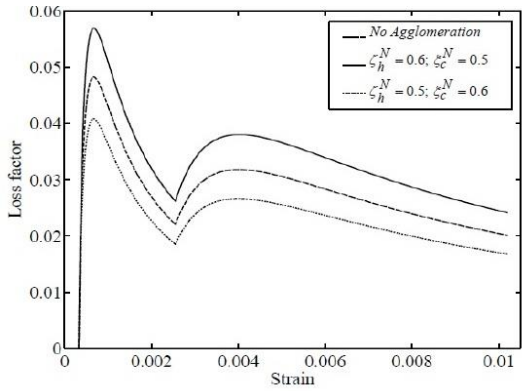

Fig. 5 Loss factor versus strain for 0.5% MWNT with $r_i = 3nm, r_o = 6.5nm$ and 5 walls

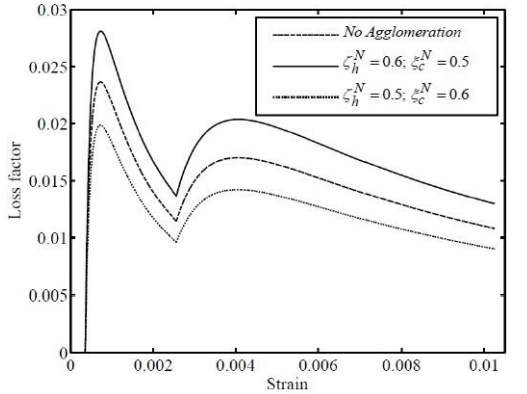

Fig. 6 Loss factor versus strain for 0.5% MWNT with $r_i = 3nm, r_o = 12nm$ and 5 walls

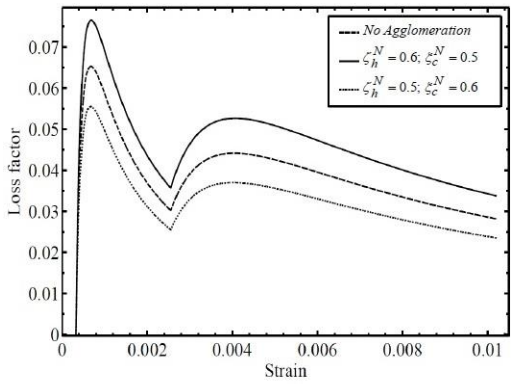

Fig. 7 Loss factor versus strain for 0.7% MWNT with $r_i = 3nm, r_o = 6.5nm$ and 5 walls

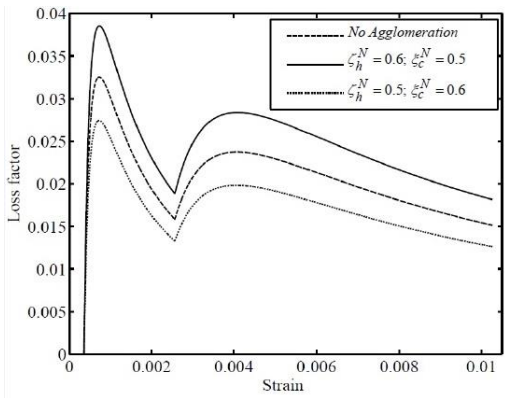

Fig. 8 Loss factor versus strain for 0.7% MWNT with $r_i = 3nm, r_o = 12nm$ and 5 walls

It may be observed that for high agglomeration having CNT volume fraction of 60%, the loss factor is increased with increase in strain amplitudes as compared to the case of no agglomeration. However, as the case is reversed that is when the CNT agglomeration is lower with 50% and the agglomeration volume fraction is higher with 60%, the loss factor decreases as compared to the situation when CNTs are not agglomerated. This effect may be due to the fact that when CNTs are highly agglomerated $(\zeta_h^N = 0.6)$ there is a strong frictional interconnectivity between the CNT layers. This results in the higher work done to move the CNTs so that the slippage occurs. As a result more amount of potential energy is stored which now results in the increase in the loss factor. Similar observations have been noticed for 0.7% weight of CNTs as shown in Figs. 7 and 8. The computed Loss factors for the nanocomposites as function of strain amplitudes may be used for validation with experimental results.

3.2 Effect of number of CNT walls

The simulations as shown in Figs. 9 and 10 indicate that as the number of CNT walls is increased, the loss factor also increases for the corresponding strain amplitudes. This increase in the loss factor occurs owing to more slippages for higher weight percentages. This may be attributed to the quantified slippage between each wall, which increases the required energy to do work that is slippage between CNT walls. A comparison of Figs. 5 and 9 shows that for the same weight percentage and CNT radius, an increase in the CNT walls by two numbers would result in an increase in the loss factor by nearly 3%. This similarity is also observed for the Figs. 7 and 10, a nearly 4% increase in loss factor is achieved due to higher CNT weight percentage (0.7%). Another important finding that may be observed from Figs. 9 and 10 is that the decrease in loss factor at the end of strain amplitude is lower for higher CNT weight fraction and higher number of CNT walls. This means that higher internal energy can be stored in the nanocomposites when the number of CNT walls is increased. Next, the variation in the loss factor due to increase in the agglomeration volume fraction from 40% to 70% has been shown in Fig. 11.

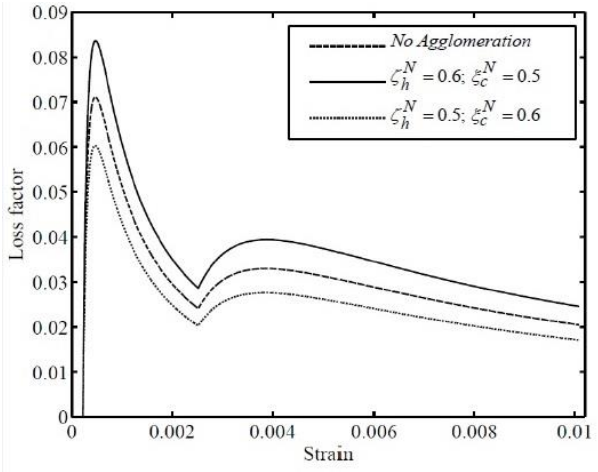

Fig. 9 Loss factor versus strain 0.5% MWNT with $r_i = 3nm, r_o = 6.5nm$ and 7 walls

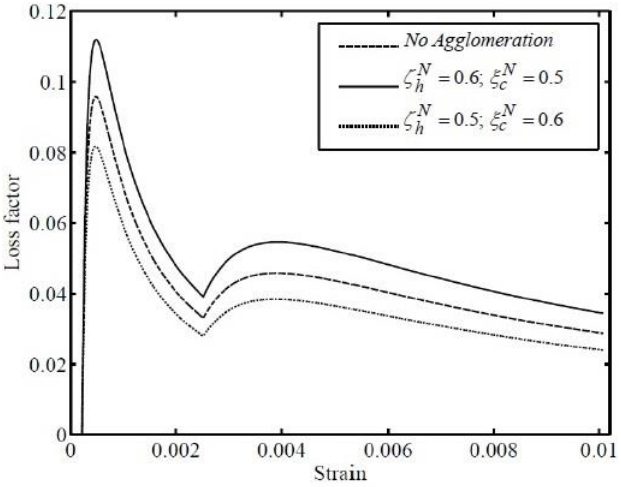

Fig. 10 Loss factor versus strain for 0.7% MWNT with $r_i = 3nm, r_o = 6.5nm$ and 7 walls

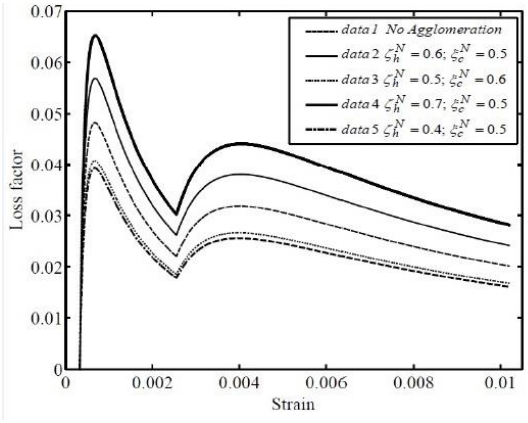

Fig. 11 Loss factor versus strain for 0.5% MWNT with $r_i = 3nm, r_o = 6.5nm$ and 5 walls

It may be observed that the agglomeration of CNTs results in additional interfacial shear stresses between the outer walls of CNTs. As a result more slippage has to be overcome which results in increased damping. The present models in literature do not take into account the agglomeration effect, and as such have limited the CNT to a weight percentage to less than 2%. However, the effective composite stiffness may be reduced under CNT agglomerations. Therefore, optimum weight fraction of CNTs with acceptable agglomeration weight fraction needs to be experimentally evaluated before obtaining higher loss factors with increasing CNT weight percentages.

3.3 Effect of interfacial shear stress and elastic modulus

The effect of change in the interfacial shear stress, which is due to the slippages between the walls in a CNT and between the CNT and the matrix, on the loss factor of the nanocomposites has also been studied. First the effect of increasing the interfacial shear stress $\tau_{2_t}^N$ from 0.3 MPa to 0.5 MPa without any CNT agglomeration has been presented in Fig. 12. It may be observed that when the critical shear stress between the walls of the CNTs $\tau_{2_t}^N$ is increased the loss factor value remains nearly the same at the start of slippage. However as the strain amplitude value increases resulting in the load transfer, the amount of potential energy does not reduce much as compared to lower shear stress value of 0.3 MPa. As a result of this stored energy, the strain amplitude value required for the next slippage between the CNT walls is achieved at a much lower value of strain amplitudes (less than 0.002 for shear stress value of 0.3 MPa). This physically implies that as the interfacial bonding between CNT walls increases higher damping may be achieved at low strain amplitude values. Next, the effect of increase in the interfacial shear stress between the CNTs $\tau_{2_t}^N$ under CNT agglomeration is shown in Fig. 13. It is observed that for dilute agglomeration although there is no decrease in loss factor, there is an improvement in the storage of potential energy, which is achieved at lower strain amplitudes. A similar result for the increase in the interfacial shear stress between CNTs and the polymer matrix $\tau_{1_P}^N$ is shown in Fig. 14. However it may be observed that with the increase in $\tau_{1_P}^N$ from 1 MPA to 1.5 MPa the amount of potential energy that may be stored is marginally higher and also the strain amplitude at which this is achieved is also higher. Therefore it may be understood that the increase in the bonding between the CNTs and resin would significantly affect the damping behavior of nanocomposites when compared to the bonding between the CNT walls themselves. Further, the previous results also provide an insight when single walled carbon nanotubes are used instead of MWCNTs. It is observed that the slippage between the CNT and resin may commence at higher values of strain amplitudes than that in the case of MWCNT walls. This may be due to the fact that the bonding between SWCNTs and the matrix is higher in comparison to the Vander Waal forces that exist among the CNT walls in case of MWCNTs.

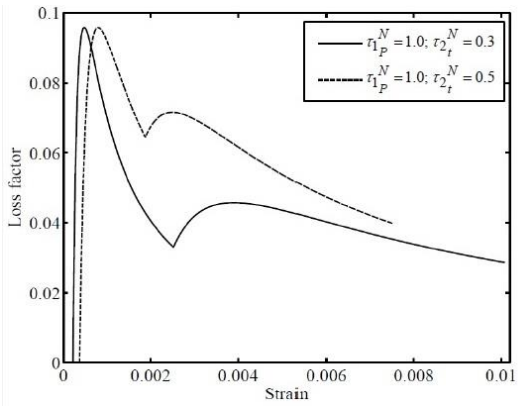

Fig. 12 Loss factor versus strain 0.7% MWNT with $r_i = 3nm, r_o = 6.5nm$ and 7 walls without agglomeration and change in shear stress values

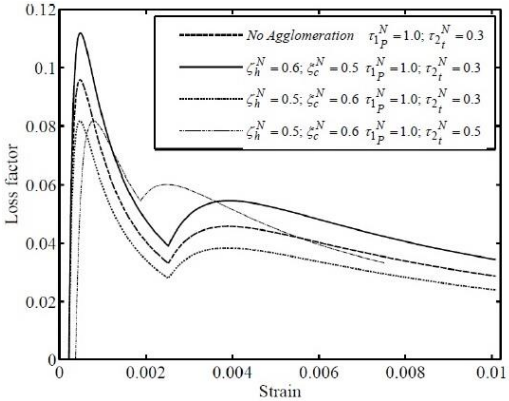

Fig. 13 Loss factor versus strain 0.7% MWNT with $r_i = 3nm, r_o = 6.5nm$ and 7 walls with agglomeration and change in shear stress value $\tau_{2_t}^N = 0.5$

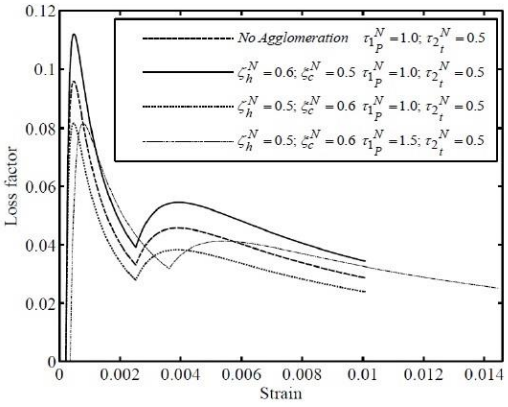

Fig. 14 Loss factor versus strain 0.7% MWNT with $r_i = 3nm, r_o = 6.5nm$ and 7 walls with agglomeration a change in shear stress value $\tau_{1_P}^N = 1.5$

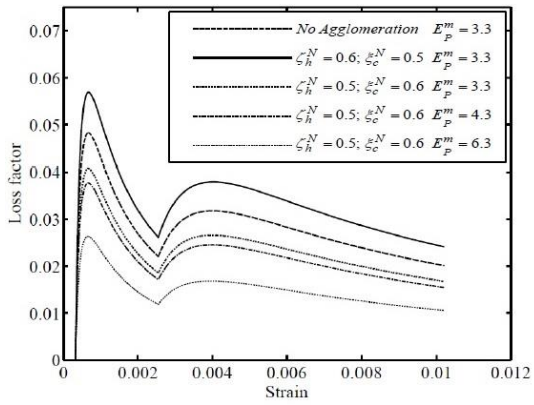

Fig. 15 Loss factor versus strain for 0.5% MWNT with $r_i = 3nm, r_o = 6.5nm$ and 5 walls $\tau_{1_P}^N = 1.5, \tau_{2_t}^N = 0.3$ with agglomeration

Since the bonding between the CNT walls and the matrix is critical, the effect of the modulus of the matrix on the damping behavior is also important, which is shown in Fig. 15. As the modulus of the matrix is increased the stiffness of the RVE of the nanocomposite also increases. In the suitable manner, decrease in the matrix modulus decreases the overall stiffness of the nanocomposite. Consequently, as stiffness is increased the damping is reduced and when stiffness is decreased damping is increased. However, a design balance should be made on the matric modulus so that both desired damping and strength of the nanocomposite can be achieved for structural applications.

4. Conclusions

The damping behavior of the nanocomposites filled with multiwalled carbon nanotubes has been studied by considering the CNT agglomerations. The proposed work presents the damping behavior for three regions of CNT agglomerations. The loss factor as a function of the strain amplitude has been computed for the high and dilute agglomeration regions. The significance of variation in the CNT weight percentages and CNT radius, the number of CNT walls, and the interfacial shear stress between the CNT walls and CNT-epoxy interface have been extensively reported. It is concluded that high CNT agglomeration increases the damping due to interconnectivity of CNT networks but reduces the mechanical and other effective properties. The dilute agglomeration not only reduces the damping but also results in poor effective properties. It is also brought out that uniform dispersion with high interfacial bonding between CNTs and the matrix provides a better combination for developing nanocomposites with good damping capabilities. Alternatively, since high agglomeration may provide improved damping this condition may be used by developing nanocomposites with additional fibers. That is, microfibers such as carbon fibers may be used as inclusions to improve the effective properties such as hygro-thermo-elastic properties of nanocomposites. The non-uniform dispersion and the random orientation can be included in the modeling procedures using micromechanics approaches. These improvements require advanced experimental setups and fabrication techniques as well as analytical modeling of effective property estimation before proposing a damping model.

References

Ajayan, P.M., Suhr, J. and Koratkar, N. (2006), "Utilizing interfaces in carbon nanotube reinforced polymer composites for structural damping", *J. Mater. Sci*., **41**(23), 7824-7829.

Arash, M., Jafar, J., Alireza, K., Tcharkhtchi, A. and Mohajeri, A. (2010), "Mechanical properties of multi-walled carbon nanotube/epoxy composites", *Mater. Design*, **31**(9), 4202-4208.

ASTM E756-05 (2010), *Standard Test Methods for Measuring Vibration Damping Properties of Materials*, Building Standards.

Buldum, A. and Lu, J.P. (1999), "Atomic scale sliding and rolling of carbon nanotubes", *Phys. Rev. Lett*., **83**, 5050-5053.

Brackbill, C.R., Lesieutre, G.A., Smith, E.C. and Ruhl, L.E. (2000). "Characterization and modeling of the low strain amplitude and frequency dependent behavior of elastomeric damper materials", *J. Am. Helicopter Soc.*, 45(1), 34-42.

Deng, C.F., Wang, D.Z., Zhang, X.X. and Ma, Y.X. (2007), "Damping characteristics of carbon nanotube reinforced aluminum composite", *Mater. Lett*., **61**(14-15), 3229-3231.

Esawi, A.M.K. and Farag, M.M. (2007), "Carbon nanotube reinforced composites: Potential and current challenges", *Mater. Design*, **28**(9), 2394-2401.

Fereidoon, A., Kordani, N., Ahangari, M.G. and Ashoory, M. (2010), "Damping augmentation of epoxy using carbon nanotubes", *Int. J. Polym. Mater*., **60**(1), 11-26.

Gou, J., Minaie, B., Wang, B., Liang, Z. and Zhang, C. (2004), "Computational and experimental study of interfacial bonding of single-walled nanotube reinforced composites", *Comp. Mater. Sci*., **31**(3-4), 225-236.

Geng, Y., Liu, M.Y., Li, J., Shi, X.M. and Kim, J.K. (2008), "Effects of surfactant treatment on mechanical and electrical properties of CNT/epoxy nanocomposites", *Compos. Part A – Appl. S.*, **39**(12), 1876-1883.

Jarali, C.S., Patil, S.F. and Pilli, S.C. (2013), "Hygro-thermo-electric properties of CNT nanocomposites with agglomeration effects. mechanics of advanced materials and structures", (DOI 10.1080/15376494.2013.769654).

Jarali, C.S., Basavaraddi, S.R., Björn, K., Pilli, S.C. and Lu, Y.C. (2014), "Modelling of the effective elastic properties of multifunctional CNT nanocomposites due to agglomeration of straight circular CNT fibers in a polymer matrix", *J. Appl. Mech. -T ASME*, **81**, 021010-1-021010-11. (Doi: 10.1115/1.4024414).

Jarali, C.S., Patil, S.F., Pilli, S.C., Raja, S. and Karjinni, V.V. (2015), "Modelling the hygro-thermo-mechanical agglomeration relations of carbon-epoxy hybrid nNanocomposites", *J. Multiscale Comput. Eng.*, **13**(3), 231-248.

Koratkar, N., Wei, B.Q. and Ajayan, P.M. (2002), "Carbon nanotube films for damping applications", *Adv. Mater*., **14**(13-14), 997-1000.

Koratkar, N.A., Suhr, J., Joshi, A. et al. (2005), "Characterizing energy dissipation in single-walled carbon nanotube polycarbonate composites", *Appl. Phys. Lett*., **87**(6), 063102.

Kireitseu, M., Hui, D. and Tomlinson, G. (2008), "Advanced shock-resistant and vibration damping of nanoparticle-reinforced composite material", *Compos. Part B - Eng*., **39**(1), 128-138.

Khan, S.U., Li, C.Y., Siddiqui, N.A. and Kim, J.K. (2011), "Vibration damping characteristics of carbon fiber-reinforced composites containing multi-walled carbon nanotubes", *Compos. Sci. Technol*., **71**(12), 1486-1494.

Lindler, J.E. and Wereley, N.M. (1999), "Double adjustable shock absorbers using electro- rheological fluid", *J. Intel. Mat. Syst. Str*., **10**(8), 652-657.

Li, C. and Chou, T.W. (2003), "Elastic moduli of multi-walled carbon nanotubes and the effect of van der waals forces", *Compos. Sci. Technol*., **63**(11), 1517-1524.

Liu, A., Huang, J.H., Wang, K.W. and Bakis, C.E. (2006), "Effects of interfacial friction on the damping characteristics of composites containing randomly oriented carbon nanotube ropes", *J. Intel. Mat. Syst. Str.*, **17**(3), 217-229.

Liu, A., Wang, K.W. and Bakis, C.E. (2010), "Multiscale damping model for polymeric composites containing carbon nanotube ropes", *J. Compos. Mater*., 44, 2301-2323.

Lin, R.M. and Lu, C. (2010), "Modeling of interfacial friction damping of carbon nanotube-based nanocomposites", *Mech. Syst. Signal Pr.*, **24**(8), 2996-3012.

Paradise, M. and Goswami, T. (2007), "Carbon nanotubes–production and industrial applications", *Mater. Design*, **28**(5), 1477-1489.

Rajoria, H. and Jalili, N. (2005), "Passive vibration damping enhancement using carbon nanotube-epoxy reinforced composites", *Compos. Sci. Technol*., **65**(14), 2079-2093.

Sun, C.T. and Lu, Y.P. (1995), *Vibration damping of structural elements*, Prentice Hall.

Salvetat-Delmotte, J.P. and Rubio, A. (2002), "Mechanical properties of carbon nanotubes: A fiber digest for beginners", *Carbon*, **40**(10), 1729-1734.

Suhr, J. and Koratkar, N. (2008), "Energy dissipation in carbon nanotube composites: A review", *J. Mater. Sci*., **43**(13), 4370-4382.

Wetzel, B., Rosso, P., Haupert, F. and Friedrich, K. (2006), "Epoxy nanocomposites-fracture and toughening mechanisms", *Eng. Fract. Mech*., **73**(16), 2375-2398.

Xu, X., Thwe, M.M., Shearwood, C. and Liao, K. (2002), "Mechanical properties and interfacial characteristics of carbon-nanotube-reinforced epoxy thin films", *Appl. Phys. Lett*., **81**, 2833.

Yu, M.F., Yakobson, B.I. and Ruoff, R.S. (2000), "Controlled sliding and pullout of nested shells in individual multi walled carbon nanotubes", *J. Phys. Chem. B*., **104**(37), 8764-8767.

Zhou, X., Shin, E., Wang, K.W. and Bakis, C.E. (2004), "Interfacial damping characteristics of carbon nanotube-based composites", *Compos. Sci. Technol*., **64**(15), 2425-2437.

CC